Transparent electrode of nanoscale metal film for optoelectronic devices

Illhwan Lee
Jong-Lam Lee

Transparent electrode of nanoscale metal film for optoelectronic devices

Illhwan Lee and Jong-Lam Lee*

Pohang University of Science and Technology, Department of Materials Science and Engineering, Hyojadong, Namgu San 31, Pohang, Gyeongbuk 790-784, Republic of Korea

Abstract. This paper reviews the principles, impediments, and recent progress in the development of ultrathin flexible Ag electrodes for use in flexible optoelectronic devices. Thin Ag-based electrodes are promising candidates for next-generation flexible transparent electrodes. Thin Ag-based electrodes that have a microcavity structure show the best device performance, but have relatively low optical transmittance (OT) due to reflection and absorption of photons by the thin Ag; this trait causes problems such as spectral narrowing and change of emission color with viewing angle in white organic light-emitting diodes. Thinning the Ag electrode to < -10 nm thickness (ultrathin Ag) is an approach to overcome these problems. This ultrathin Ag electrode has a high OT, while providing comparable sheet resistance similar to indium tin oxide. As the OT of the electrode increases, the cavity is weakened, so the spectral width of the emission and the angular color stability are increased. © *2015 Society of Photo-Optical Instrumentation Engineers (SPIE)* [DOI: 10.1117/1.JPE.5.057609]

Keywords: ultrathin; flexible; transparent electrode; Ag; organic light-emitting diode.

1 Introduction

Transparent conducting oxides (TCOs) can be used as transparent electrodes for various optoelectronic devices, such as organic light-emitting diodes (OLEDs) and organic solar cells (OSCs).[1–9] Indium tin oxide (ITO) is widely used as a TCO due to its high optical transmittance (OT ~90%) and good conductivity (sheet resistance $R_s < 20 \ \Omega/\square$).[10–12] However, ITO film has limitations due to its high growth temperature, high cost, and poor mechanical flexibility.[13,14] Furthermore, ITO films are obtained using sputtering techniques, which can damage the underlying layers.[15,16] Thus, significant research has been directed toward finding a suitable replacement for ITO. Nanostructured conducting materials such as Ag nanowires,[17,18] graphenes,[19] poly (3, 4-ethylenedioxythiophene) poly(styrenesulfonate) (PEDOT:PSS),[20] metal grids,[21–25] ITO nanobranch,[26,27] and ZnO-doped In_2O_3[28] have been evaluated as flexible electrodes to overcome the shortcomings of ITO. Metal nanowires show high transmittance (~86%) and relatively low sheet resistance (~16 $\Omega/\square$), but poor thermal stability and rough surface morphology causing poor efficiency.[29,30] Graphene, PEDOT:PSS, and ITO nanobranch have superior flexibility, but are limited by low conductivity and lack of uniformity in large areas.[20,26,31] Metal grids have also been used for transparent electrodes, with excellent conductivity and flexibility. However, fabrication procedures are high cost and complex.[21]

One way to produce a transparent electrode is to incorporate a thin metal electrode. Metal/dielectric and dielectric/metal/dielectric structures combine the characteristics of high electrical conductivity of metals and good mechanical ductility of thin films.[32–37] However, these structures have relatively low OT ~80%. Ultrathin Ag electrodes are promising for this function because the OT and R_s of these electrodes are comparable to or better than those of ITO

---

electrodes.[38–49] In addition, their mechanical properties are appropriate for use in flexible devices.[40] This review highlights recent progress in the fabrication of nanoscale thin Ag electrodes. It includes an introduction on the relevant theory and detailed discussion of the characteristics of ultrathin Ag film. To clarify the trends in ultrathin Ag electrode development, we organize them according to the methods used to form ultrathin Ag films.

2 Ag Electrodes for Organic Electronics

Several studies have considered applications of Ag film to the electrode of organic electronics. Ag has the highest OT and lowest R_s among metals, and is ductile.[50,51,52] However, even though Ag has a high OT compared to other metals, a thin film of Ag (>10 nm) has a low OT compared to ITO film.[53] Therefore, most Ag electrodes are used as semitransparent electrodes. Use of a semitransparent electrode can cause a microcavity effect, which improves the optical property of devices.[50,54] Destructive interferences within the microcavity reduce the internal reflection of OLEDs. Ultrathin Ag electrodes are promising for this function because of OTs and R_ss that are comparable to or better than those of ITO electrodes.[50] The optical enhancement ratio varies according to metal film and dielectric material [Fig. 1(a)]. To maximize the microcavity effect, the thickness of each layer should be designed optically.[54] Thin Ag electrodes can achieve an OSC performance that exceeds those of OSCs with ITO electrodes.[50] The thickness of the active layer can be adjusted to maximize the electric field within the active layer [Fig. 1(b)]. The resulting microcavity resonant condition amplifies the electric field within the cell to give a higher performance than the ITO-based devices. Although microcavity effects can increase the device efficiency, its OT is degraded due to reflection and absorption by the Ag electrodes. Therefore, a microcavity is not appropriate for transparent displays, lighting, or solar cells. The irradiance that has been absorbed is given by the difference between the irradiance I_{in} incident on the thickness element and the irradiance I_{ext} that emerges from the exit side.[55] The irradiance absorbed by a layer is given by[55]

$$I_{abs} = \frac{2\pi}{\lambda} nkd\gamma |E^2|,$$

where E is the average amplitude of the electric field in the film considered, γ is the free-space admittance, λ is the wavelength of irradiance, n is the refractive index, k is the extinction coefficient, and d is the optical thickness. This equation demonstrates that I_{abs} can be decreased (OT can be increased) by reducing nk. ITO has a low nk. But among metals, only Ag and Au have a suitably low nk.[27]
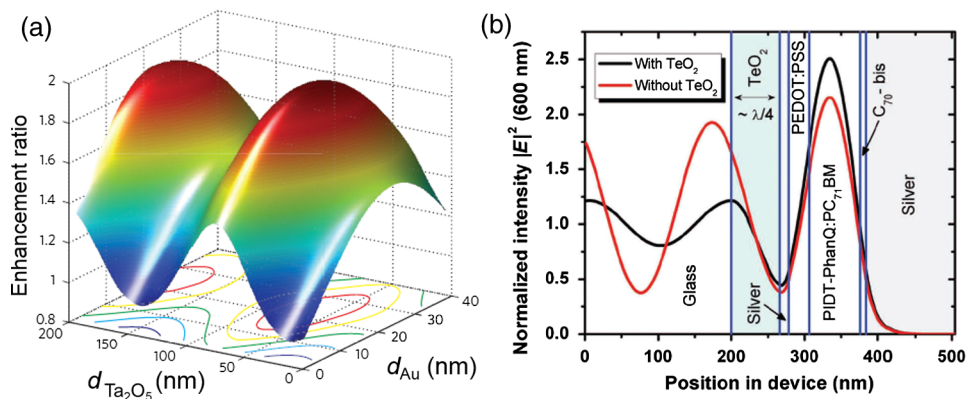

Fig. 1 (a) Calculated enhancement ratio of the $Ta_2O_5/Au/MoO_3$ electrode relative to indium tin oxide as a function of the thickness of both Au and Ta_2O_5.[54] Reprinted with permission from Ref. 54. Copyright 2012, Nature Publishing Group. (b) Electric field calculated by transfer matrix method considering a unitary incoming intensity for a 600 nm light wave (incident from the left).[50] Reprinted with permission from Ref. 50. Copyright 2013, Wiley-VCH.

To maximize the OT of the Ag film, it must be as thin as possible. Generally, an OLED with an Ag electrode >10-nm thick shows a narrow emission spectrum due to the strong cavity effect, and a weak intensity contribution in the undesigned wavelength region. Furthermore, emission color changes with the viewing angle. Therefore, Ag electrodes >10-nm thick are not good for broad wavelength range applications such as white OLEDs. Several approaches to use an ultra-thin (<10 nm) Ag electrode have been reported.[38–49] As the OT of the electrode increases, its emission spectrum broadens, in agreement with theoretical expectations for a weak microcavity.[56] Using a weak microcavity also increases the angular color stability and the device efficiency.[44]

3 Fundamental Principle on Conduction and Transmittance of Thin Ag Film

Agglomeration (growth of "islands") is a transport process that reduces the overall energy of a system.[57] In most heteroepitaxial systems, films grown on a foreign substrate energetically favor island growth and thus are subject to dewetting instability.[58] This means that the interaction between substrate and Ag atoms is an important factor to determine the growth mode. Depending on the interaction energies of substrate atoms and film atoms, any of three growth modes (Frank-van der Merwe mode, Volmer-Weber mode, Stranski-Krastanov mode) can occur (Fig. 2).[59] Layers of material grow one on top of another: this is called layer-by-layer growth (Frank-van der Merwe mode). Interaction between substrate and atoms in a film is greater than the distance between adjacent atoms in the film (Fig. 2). Ag layers exhibit three-dimensional (3-D) island growth (Volmer-Weber mode) as a result of the poor wettability of Ag on the substrate. Ag films have very low adhesion energy at the metal/oxide interface:[60] this means that the Ag atoms interact more strongly with each other than with the substrate. Therefore, Ag films tend to form islands on the substrates; this process yields a rough and discontinuous surface.

A discrete Ag film that consists of islands strongly absorbs and scatters light because of localized surface plasmon resonance (LSPR).[39,61] LSPR results from the coupling between incident light and the free electron gas at the surface of a metal island structure.[62] Coupling between light and free electron causes some light to be absorbed and some to be scattered. This coupling occurs at specific frequencies for each kind of metal. Ag has its LSPR frequency in the visible wavelength region. Glass/Ag samples show specific dips related to LSPR at wavelengths near 500 nm [Fig. 3(a)]. Simulations and experimental results did not match at a low Ag thickness because Ag film <10-nm thick has many isolated clusters and voids. The R_s of Ag on the bathocuproine increases as Ag thickness T_{Ag} decreases [Fig. 3(b)] due to island growth of the Ag film, and R_s is infinite at $T_{Ag} < 6$ nm. The isolated metallic grains provide no sufficient conductive paths through the layer. However, after the percolation threshold is reached, separate metal islands start to connect and form a continuous layer: this process causes R_s to decrease rapidly.[63] To obtain a highly conductive and transparent Ag film, it must be continuous and smooth.

4 Recent Methods for Formation of Ultrathin Ag Film

4.1 *Seed Layer*

The island growth of Ag occurs because the substrate has low surface energy compared to Ag ($\gamma = 1.25 \text{ J m}^{-2}$).[64] The introduction of seed layers reduces the difference in γ between
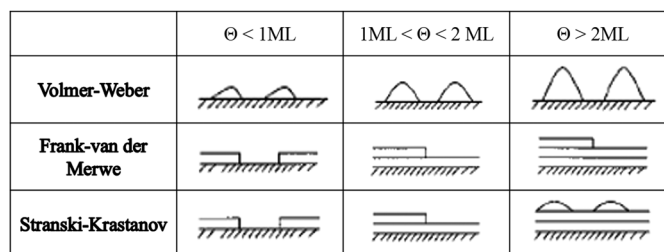
	$\Theta < 1\text{ML}$	$1\text{ML} < \Theta < 2\text{ML}$	$\Theta > 2\text{ML}$
Volmer-Weber			
Frank-van der Merwe			
Stranski-Krastanov			

Fig. 2 Initial states of film growth. Θ, substrate surface coverage in monolayers (MLs).[59] Reprinted with permission from Ref. 59. Copyright 2015, The Optical Society.
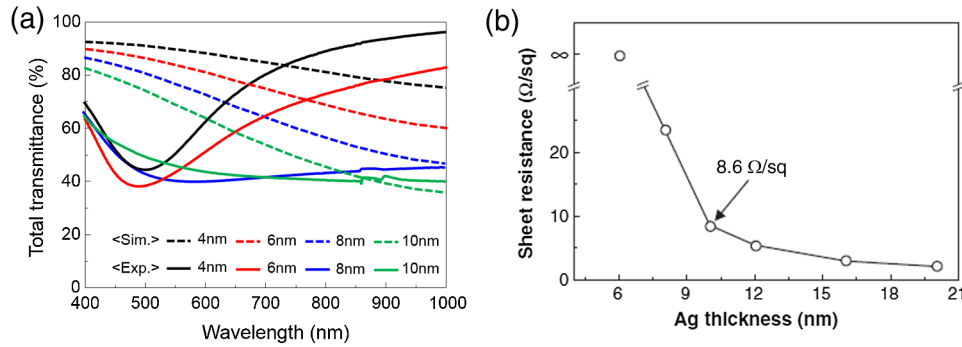
Fig. 3 (a) Total transmittance of the glass/Ag films as a function of Ag thickness (dotted line: simulation, solid line: experimental results). Commercial thin film simulator is used for simulation (The Essential Macleod, Thin Film Center Inc.) (b) Sheet resistance of Ag on BCP as a function of various Ag thicknesses.[63] Reprinted with permission from Ref. 63. Copyright 2013, Wiley-VCH.

the substrate and Ag. Wetting of Ag layer on the substrate is significantly improved by adding seed materials such as Au, Al, Ca, Ge, Ni, MoO_3, or Cs_2CO_3.[38–46] A Ca seed layer with $\gamma = 0.5 \, J \, m^2$, and an Al seed layer with $\gamma = 1.15 \, J \, m^{-2}$ reduce the difference in γ between the substrate and Ag.[39] Schubert et al.[39] obtained a continuous and smooth 7-nm thick Ag film using an Au seed layer. Because Au has a higher $\gamma (= 1.5 \, J \, m^{-2})$ than does Ag, the attachment of Ag atoms to the Au surface is favored over agglomeration [Fig. 4(a)]. For a nominal thickness <7 nm, glass/Ag samples have a low OT and high R_s [Fig. 4(b)].[38] The use of an Au seed layer causes the morphology of the Ag film to become very smooth and homogeneous, even for total thickness of the Ag layer <10 nm. Compared to ITO, the Ag film with an Au seed layer has a similar OT and lower R_s [Fig. 4(b)].
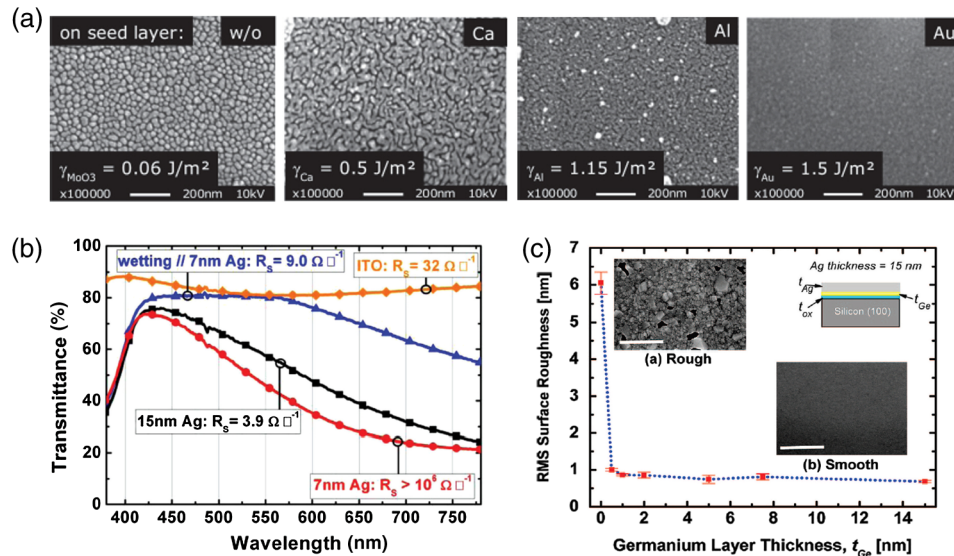

Fig. 4 (a) Scanning electron micrographs of 7-nm thick silver layers deposited on p-doped N, N′-((diphenyl-N, N′-bis)9,9,-dimethyl-fluoren-2-yl)-benzidine which mimics the organic solar cell (OSC) and various seed layers with different surface energies γ taken from literature. The white scale bar represents 200 nm.[39] Reprinted with permission from Ref. 39. Copyright 2013, Wiley-VCH. (b) Transmittance and sheet resistance of the different transparent electrodes are investigated here.[38] Reprinted with permission from Ref. 38. Copyright 2013, Wiley-VCH. (c) Plot showing the average root mean square (RMS) surface roughness as a function of Ge thickness for a constant Ag thickness of 15 nm. The insets (a) and (b) show the contrast between a rough and a smooth surface for SEM images of without and with Ge (scale bar: 0.5 μm).[65] Reprinted with permission from Ref. 65. Copyright 2009, American Chemical Society.

Seed layers such as Ge and $CsCO_3$ promote nucleation of Ag.[46,66] Williams et al. used a Ge seed layer to achieve a continuous Ag film.[65] Although the Ge deposition on the substrate also caused island growth, the density of the Ge nuclei was much larger and the islands were significantly smaller than those for Ag deposited without a seed layer on the substrate. This surface provided a heterogeneous nucleation site for the deposited Ag atoms. The activation energy for Ag diffusion is ~0.45 eV on a Ge surface and ~0.32 eV on a SiO_2 surface.[67] Therefore, using a Ge seed layer before depositing Ag reduces the surface diffusion and mass transportation of Ag, and results in a smooth and continuous Ag film. Compared to the topology between rough and smooth [Fig. 4(c), inset], without the layer of Ge, the deposited Ag formed distinct polycrystalline granular clusters with irregular shapes and a significant density of pinholes, which made the film electrically discontinuous. However, a Ge seed layer with thickness >0.5 nm leads to a suppression of Ag island growth, thereby smoothing the film. The smoother Ag thin films also had a lower sheet resistance ($R_{s,Rough} \sim 40$ $\Omega/\square$, $R_{s,Smooth} \sim 20$ $\Omega/\square$).[65] Metal and oxide can be used as good wetting layers in all device structures.

4.2 Surface Treatment

The growth of Ag islands can also be reduced by derivatizing the substrate with a layer of molecules designed to enhance Ag nucleation by interacting strongly with both the substrate and the incoming Ag atoms.[68] Zou et al.[69] improved the Ag wetting property by applying a double-end functionalized 11-mercapto-undecanoic acid (MUA) self-assembled monolayer (SAM) on the substrate as a molecular binder to covalently attach Ag to the substrate. In the absence of a seed layer, discontinuous Ag islands grow on a glass substrate [Fig. 5(a)], but MUA can interact with the incident Ag atoms to form an ester linkage which minimizes surface diffusion and enhances Ag nucleation, so the Ag film is very smooth with a low root mean square roughness and reduced R_s [Fig. 5(b)]. However, lauric acid SAM has an inert $-CH_3$ terminal group which leads to a significantly rough surface due to the growth of Ag islands [Fig. 5(c)]. To maximize the adhesion between the substrate and Ag, the appropriate SAM material must be chosen.

4.3 Low-Temperature Deposition

Temperature can affect the growth of Ag islands. Even dewetting has been observed when the temperature exceeds 102°C.[70,71] Ultrathin continuous Ag films are produced at low temperatures. A low substrate temperature generally reduces surface diffusion of Ag atoms, and thus alters the nucleation processes.[72] Presland et al.[73] defined induction time t_i as the time at which the void density increases in the film during an isothermal anneal for a given film thickness; it is related to the activation energy E_{ai} of void formation as
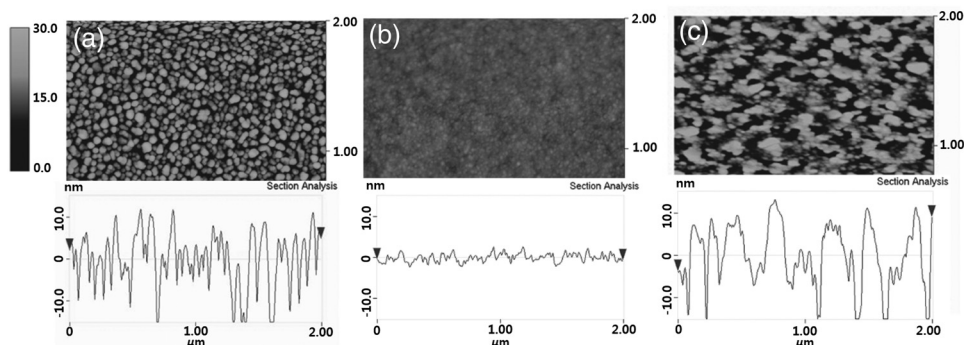

Fig. 5 AFM images of 10-nm ultrathin Ag films on top of (a) glass (surface roughness RMS = 6.07 nm, sheet resistance = N/A), (b) glass/ZnO/MUA (surface roughness RMS = 0.95 nm, sheet resistance = 8.61 $\Omega/\square$), and (c) glass/ZnO/lauric acid (surface roughness RMS = 9.38 nm, sheet resistance = 10.87 $\Omega/\square$).[69] Reprinted with permission from Ref. 69. Copyright 2014, Wiley-VCH.

$$t_i = A \, \exp\frac{E_{ai}}{kT},$$

where A is a pre-exponential factor, k is the Boltzmann constant, and T is the absolute annealing temperature. E_{ai} is comparable to that reported in the literature for the surface diffusion activation energy of an Ag thin film in a vacuum.[74] Therefore, to reduce Ag agglomeration, E_{ai} should be increased and T should be decreased. Sergeant et al.[75] optimized several deposition parameters to minimize the growth of Ag islands by controlling the evaporation rate and substrate temperature. The best results were obtained at a deposition rate of 5.5 to 6 Å/s onto a substrate cooled to −5°C. Increasing the evaporation rates and reducing the substrate temperature caused a reduction in the surface diffusion of Ag atoms: this means that sufficient nucleation sites are created to enhance the lateral growth of Ag films. Although a low-temperature process may be useful for the growth of ultrathin Ag layers, the process cost is high due to the requirement of the equipment needed to maintain a low temperature.

4.4 Doping Effect

In a nonwetting system, flat ultrathin Ag films tend to transform to 3-D islands.[76] This dewetting tendency of pure Ag becomes more obvious at elevated temperatures.[57,77] Zhang et al.[48] and Gu et al.[49] used Al doping to fabricating ultrathin (3 nm) Ag-based thin films with high thermal stability on SiO_2/Si (100) substrates. Al doping yielded smaller and denser nuclei [Fig. 6(a)] than those in pure Ag films [Fig. 6(b)]: this difference reveals that Al doping causes an increase in the nuclei density of the films. Al-O bonds are much stronger than Ag-O bonds[60] so Al atoms are immobilized on the substrate and can hinder the diffusion of Ag atoms; therefore, Al-doping causes increased spatial density of nuclei and reduced size of particles. Figures 6(c) and 6(e) show the SEM images of 15 nm as-deposited pure Ag and Al-doped Ag films. Due to dewetting, pure Ag film easily changes to isolated islands after annealing at 300°C [Fig. 6(d)]. In contrast, an Al-doped Ag film shows an ultrasmooth surface morphology that is very similar to that of the as-deposited surface [Fig. 6(f)]. These results show that Al doping is a very effective method to form an ultrathin Ag layer with high thermal stability. Wang et al.[47] used oxygen doping to achieve an ultrathin Ag-based film. The oxygen-doped Ag (AgO_x) layer was 6-nm thick and was completely continuous and smooth. Oxygen doping of the ultrathin Ag layer improved its OT without any noticeable degradation of electrical conductivity.

5 Application and Developments

5.1 Organic Light-Emitting Diode Lighting and Organic Solar Cell with a High Performance

Monochromatic top-emitting OLEDs based on thin metal electrodes show high efficiency due to their microcavity structure. However, as a result of spectral narrowing and change of emission color with viewing angle, white OLEDs show low efficiency and color quality.[78,79] To achieve highly efficient white OLEDs, the OT of the transparent electrode must be increased. Schwab et al.[38] used an ultrathin Ag electrode to improve the characteristics of the top electrode, and achieved better color quality and color stability compared to those of an optimized white OLED based on an ITO electrode. The highly transparent ultrathin Ag electrode increased the spectral width of the microcavity [Fig. 7(a), red line] and increased the luminous efficacy by 25% compared to a standard Ag electrode.

Wang et al.[47] demonstrated a highly transparent ultrathin Ag electrode for flexible inverted OSCs, and it achieved a higher power conversion efficiency (PCE) and external quantum efficiency (EQE) than did conventional ITO-based OCSs [Fig. 7(b)]. The PCE and EQE enhancements using an ultrathin oxygen doped AgO_x electrode were mainly the result of its increased OT [Fig. 7(b), inset]. The AgO_x electrode provided an EQE = 64% at 620 nm: this is the highest value achieved by any flexible OSC fabricated on polymer substrates.

OSCs fabricated on a thin metal electrode show enhanced PCEs due to the optical cavity effect. The method of tuning the optical cavity in a device is to change the thickness of the
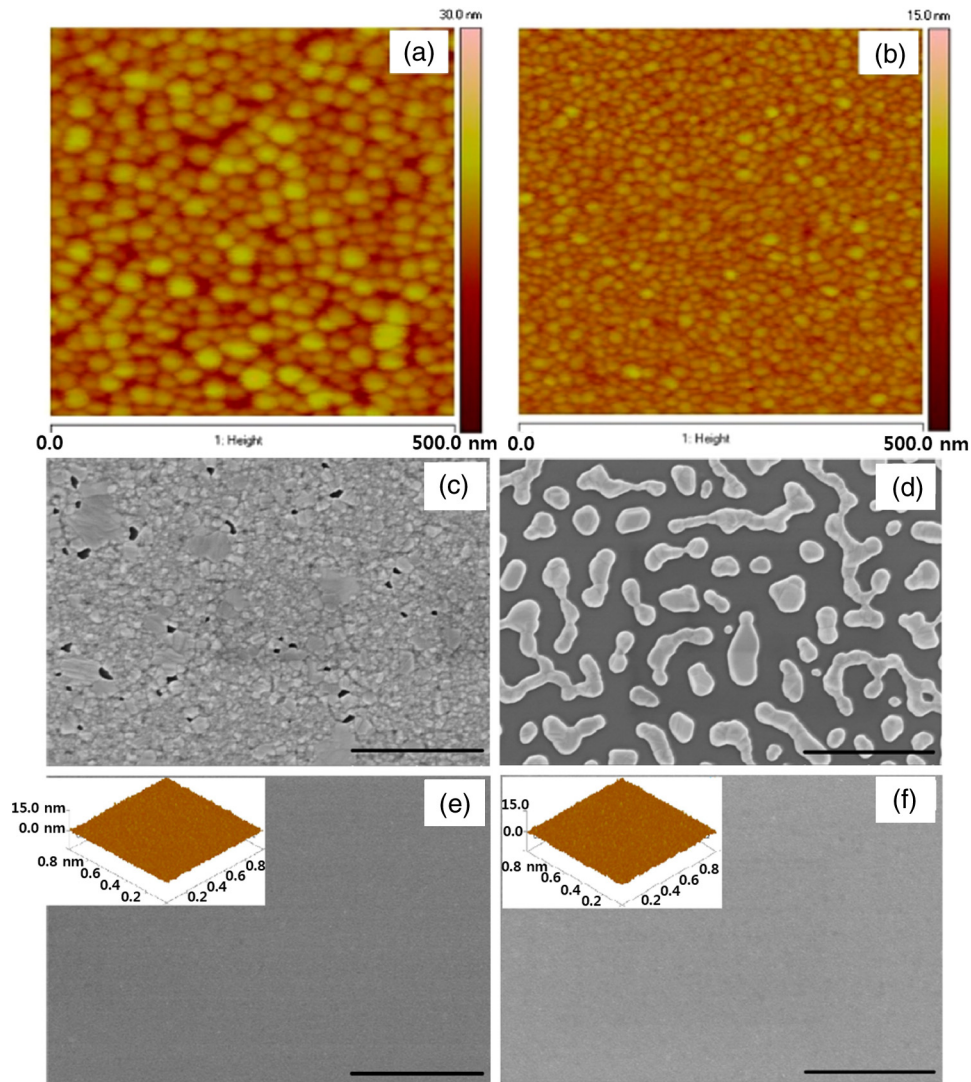
Fig. 6 Two-dimensional AFM images of (a) 3 nm pure Ag films, (b) 3 nm Al-doped Ag films on SiO$_2$/Si (100) substrates. SEMs (scale bars = 1 μm) of (c) 15 nm as-deposited and (d) annealed pure Ag films on SiO$_2$/Si in N$_2$ at 300°C (e) 15 nm as-deposited and (f) annealed Al-doped Ag films on SiO$_2$/Si in N$_2$ at 300°C. The insets in (e) and (f) are AFM images of 15 nm as-deposited and annealed Al-doped Ag films on SiO$_2$/Si with an RMS roughness of 0.43 and 0.45 nm, respectively.[49] Reprinted with permission from Ref. 49. Copyright 2014, American Chemical Society.

layers between reflective and semitransparent metal electrodes, with the objective of changing the length of the optical path.[54] Some groups have tuned the optical cavity to improve the performance of OSCs. To maximize the photocurrent, the thickness of the hole transport layer (HTL) can be optimized to the optical cavity so that the resonance frequency occurs in a spectral range in which light absorption by the absorber is weak.[75] This tuning increased the optical characteristics such as high fill factor, open circuit voltage, and PCE by up to 4.4%, so the HTLs are attractive replacements for ITO electrodes in OSCs.[75] A 7 nm Al-doped Ag-based device with a resonance cavity in the active layer between the reflective anode and the semi-transparent ultrathin Al-doped Ag cathode has a spectrum peak that is close to the absorption edge of a photoactive absorber.[48]

5.2 Flexible Device Application

ITO-based flexible optoelectronic devices show a dramatically decreased performance during bending. A flexible OSC that uses an Ag electrode with a TeO$_2$ seed layer showed stable
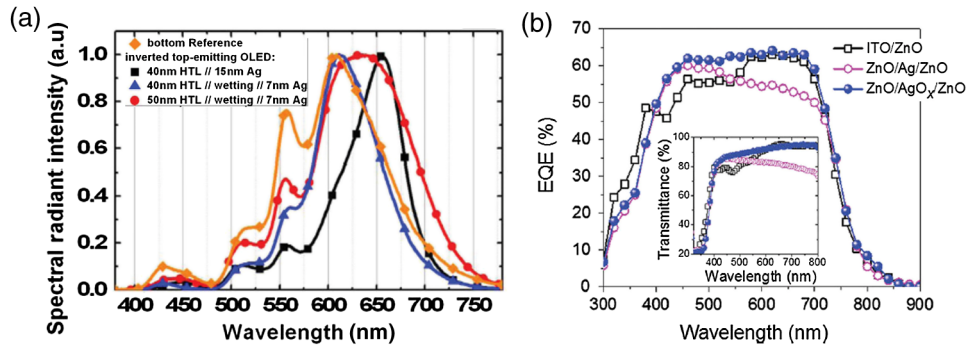
Fig. 7 (a) Normalized spectral radiant intensity measured at current density of 14.8 mA cm^{-2} for the different OLEDs investigated in this study. A hole transport layer (HTL) thickness in the wetting layer device is optimized to 50 nm.[38] Reprinted with permission from Ref. [38]. Copyright 2013, Wiley-VCH. (b) EQE spectra of OSCs using different transparent electrodes. Inset: specular transmittances.[47] Reprinted with permission from Ref. [47]. Copyright 2013, Wiley-VCH.
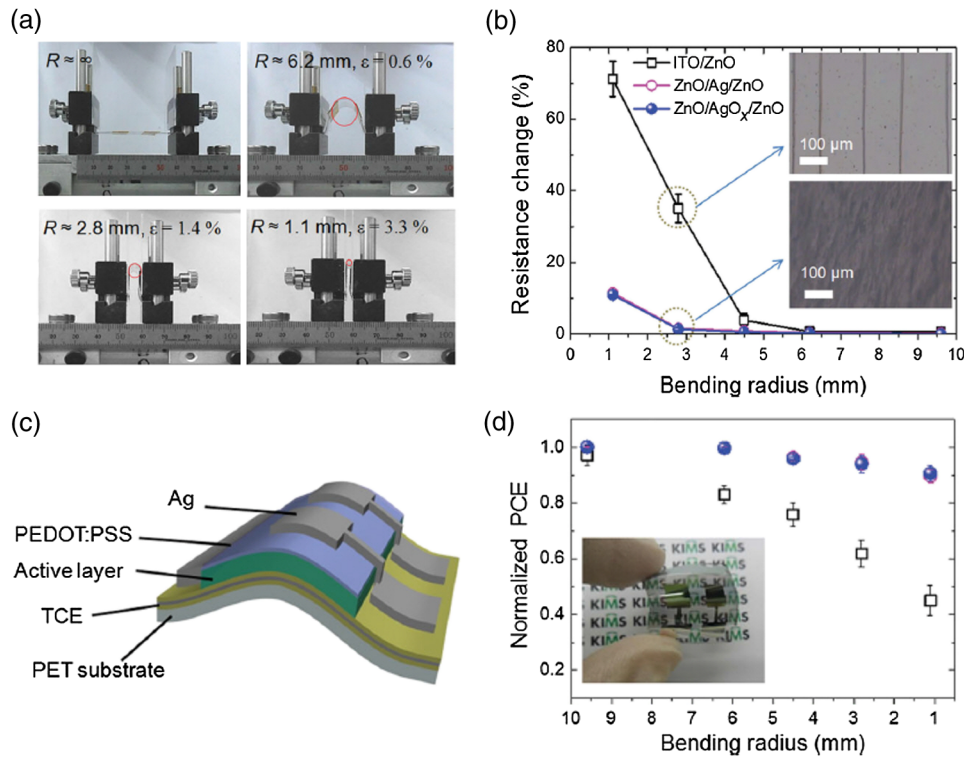

Fig. 8 (a) Photographs of irreversible bending tests of flexible transparent conducting electrodes (TCEs) coated on the polyethylene terephthalate (PET) substrates. (b) The percentage change in the resistance of the TCEs as a function of the bending radius. Insets represent the optical images of the TCEs after being bent with a bending radius of 2.8 mm. (c) Device architecture of flexible OSC fabricated on a PET substrate used in this study. (d) Power conversion efficiency values measured for flexible OSCs as a function of bending radius during compressive bending, normalized to the initial value. Inset: fabricated flexible OSC using ultrathin Ag electrode on a PET substrate.[47] Reprinted with permission from Ref. [47]. Copyright 2013, Wiley-VCH.

performance even after >100 bending cycles (radius = 0.64 cm).[50] Wang et al. demonstrated a flexible OSC that uses an ultrathin AgO$_x$ electrode [Fig. 8(a)].[47] The percentage change in R_s of the ITO electrode was 35% higher than that of the AgO$_x$ electrode at the same bending radius as a result of the formation and propagation of microscopic cracks in the ITO [Fig. 8(b), inset]. However, the R_s of the ultrathin Ag electrode changed little under bending stress, and formed no cracks on the film surface. Figure 8(c) shows the device architecture of the flexible OSC using

an ultrathin Ag electrode. As the bending radius decreased, the PCE of the ITO-based OSC greatly decreased, but that of the ultrathin Ag-based OSC was not severely affected [Fig. 8(d)]. Compared to ITO-based OSCs, the higher flexibility of the ultrathin Ag electrode ensured the superior structural durability of OSCs.

6 Summary

Ultrathin Ag electrodes are promising candidates as next-generation flexible transparent electrodes. Compared with other transparent electrodes, these ultrathin metal-based transparent electrodes have the highest OT, flexibility, and low R_s. However, growth of 3-D Ag islands causes strong absorption and scattering of incident light: because of LSPR, and these phenomena degrade its transparency. Smooth and ultrathin Ag layers (<10 nm) could be produced by introducing a seed layer, by using surface treatment, by low-temperature deposition, and by doping. The high OT of the ultrathin Ag electrode can improve the color quality and color stability of white OLEDs that use a weak microcavity structure.[38,40,44] Ultrathin Ag electrodes have been used to achieve the highest EQE of any flexible OSC fabricated on polymer substrates.[47] Ultrathin Ag-based electrodes provide opportunities to demonstrate highly flexible and transparent optoelectronic applications. However, several disadvantages of ultrathin Ag electrodes remain to be overcome; these include light absorption by the seed layer, a trade-off between OT and R_s when changing the thickness of Ag films and low thermal stability.

Acknowledgments

References

1. P. Gorrn et al., "Towards see-through displays: fully transparent thin-film transistors driving transparent organic light-emitting diodes," *Adv. Mater.* **18**(6), 738–741 (2006).
2. G. Gu et al., "Transparent flexible organic light-emitting devices," *Adv. Mater.* **9**(9), 725–728 (1997).
3. S. Reineke et al., "White organic light-emitting diodes with fluorescent tube efficiency," *Nature* **459**, 234–238 (2009).
4. W. J. Dong et al., "Effect of ultra-violet-ozone on ITO/P3HT interface for PEDOT:PSS-free polymer solar cells," *Sol. Energy Mater. Sol. Cells* **109**, 240–245 (2013).
5. K. Hong et al., "Enhanced light out-coupling of organic light emitting diodes: spontaneously formed nano-facet structured MgO as a refractive index modulation layer," *Adv. Mater.* **22**(43), 4890–4894 (2010).
6. W. J. Dong, G. H. Jung, and J.-L. Lee, "Solution-processed-MoO$_3$ hole extraction layer on oxygen plasma treated indium tin oxide in organic photovoltaics," *Sol. Energy Mater. Sol. Cells* **116**, 94–101 (2013).
7. K. Hong and J.-L. Lee, "Review paper: recent developments in light extraction technologies of organic light emitting diodes," *Electron. Mater. Lett.* **2**(1), 021215 (2012).
8. S. Loser et al., "High-efficiency inverted polymer photovoltaics via spectrally tuned absorption enhancement," *Adv. Energy Mater.* **4**(14), 1301938 (2014).
9. N. Li et al., "Environmentally printing efficient organic tandem solar cells with high fill factors: a guideline towards 20% power conversion efficiency," *Adv. Energy Mater.* **4**(11), 140084 (2014).
10. S. Reineke et al., "White organic light-emitting diodes with fluorescent tube efficiency," *Nature* **459**, 234–238 (2009).
11. R. Capelli et al., "Organic light-emitting transistors with an efficiency that outperforms the equivalent light-emitting diodes," *Nat. Mater.* **9**, 496–503 (2010).
12. D. Joly et al., "White organic light-emitting diodes based on quench-resistant fluorescent organophosphorus dopants," *Adv. Funct. Mater.* **22**(3), 567–576 (2012).

13. C. Feng et al., "Flexible, stretchable, transparent conducting films made from superaligned carbon nanotubes," *Adv. Funct. Mater.* **20**(6), 885–891 (2010).
14. J. Meyer et al., "Transparent inverted organic light-emitting diodes with a tungsten oxide buffer layer," *Adv. Mater.* **20**(20), 3839–3843 (2008).
15. S. Y. Ryu et al., "Highly efficient transparent organic light-emitting diodes by ion beam assisted deposition-prepared indium tin oxide cathode," *Appl. Phys. Lett.* **90**(3), 033513 (2007).
16. C.-H. Chung et al., "Improvement in performance of transparent organic light-emitting diodes with increasing sputtering power in the deposition of indium tin oxide cathode," *Appl. Phys. Lett.* **86**(9), 093504 (2005).
17. K. Ziberberg et al., "Highly robust indium-free transparent conductive electrodes based on composites of silver nanowires and conductive metal oxides," *Adv. Funct. Mater.* **24**(12), 1671–1678 (2014).
18. J.-W. Lim et al., "Simple brush-painting of flexible and transparent Ag nanowire network electrodes as an alternative ITO anode for cost-efficient flexible organic solar cells," *Sol. Energy Mater. Sol. Cells* **107**, 348–354 (2012).
19. S. Pang et al., "Graphene as transparent electrode material for organic electronics," *Adv. Mater.* **23**(25), 2779–2795 (2011).
20. Y. H. Kim et al., "Achieving high efficiency and improved stability in ITO-free transparent organic light-emitting diodes with conductive polymer electrodes," *Adv. Funct. Mater.* **23**(30), 3763–3769 (2013).
21. M. G. Kang and L. J. Guo, "Nanoimprinted semitransparent metal electrodes and their application in organic light-emitting diodes," *Adv. Mater.* **19**(10), 1391–1396 (2007).
22. C. Min et al., "Enhancement of optical absorption in thin-film organic solar cells through the excitation of plasmonic modes in metallic gratings," *Appl. Phys. Lett.* **96**(13), 133302 (2010).
23. M.-G. Kang et al., "Efficiency enhancement of organic solar cells using transparent plasmonic Ag nanowire electrodes," *Adv. Mater.* **22**(39), 4378–4383 (2010).
24. P. B. Catrysse and S. Fan, "Nanopatterned metallic films for use as transparent conductive electrodes in optoelectronic devices," *Nano Lett.* **10**(8), 2944–2949 (2010).
25. B. Zeng, Z. H. Kafafi, and F. J. Bartoli, "Transparent electrodes based on two-dimensional Ag nanogrids and double one-dimensional Ag nanogratings for organic photovoltaics," *J. Photon. Energy* **5**(1), 057005 (2014).
26. H. K. Yu et al., "Three-dimensional nano-branched indium-tin-oxide for organic solar cells," *ACS Nano* **5**(10), 8026–8032 (2011).
27. H. K. Yu et al., "Nano-branched transparent conducting oxide: beyond the brittleness limit for the flexible electrode applications," *Nanoscale* **4**(21), 6831–6834 (2012).
28. K. Kwak, K. Cho, and S. Kim, "Stable bending performance of flexible organic light-emitting diodes using IZO anodes," *Sci. Rep.* **3**, 2787 (2013).
29. A. Kumar and C. Zhou, "The race to replace tin-doped oxide: which material will win?," *ACS Nano* **4**(1), 11–14 (2010).
30. J.-Y. Lee et al., "Solution-processed metal nanowire mesh transparent electrodes," *Nano Lett.* **8**(2), 689–692 (2008).
31. J. O. Hwang et al., "Work function-tunable, n-doped reduced graphene transparent electrodes for high-performance polymer light-emitting diodes," *ACS Nano* **6**(1), 159–167 (2012).
32. D. Poitras, C.-C. Kuo, and C. Py, "Design of high-contrast OLEDs with microcavity effect," *Opt. Express* **16**(11), 8003–8015 (2008).
33. M. Thomschke et al., "Optimized efficiency and angular emission characteristics of white top-emitting organic electroluminescent diodes," *Appl. Phys. Lett.* **94**(8), 083303 (2009).
34. P. Freitag et al., "White top-emitting organic light-emitting diodes with forward directed emission and high color quality," *Org. Electron.* **11**(10), 1676–1682 (2010).
35. K. Hong et al., "Optical properties of $WO_3/Ag/WO_3$ multilayer as transparent cathode in top-emitting organic light emitting diodes," *J. Phys. Chem. C* **115**(8), 3453–3459 (2011).
36. J. Y. Ham et al., "Design of broadband transparent electrodes for flexible organic solar cells," *J. Mater. Chem. A* **1**(9), 3076–3082 (2013).

37. S. Kim et al., "MgO nano-facet embedded silver-based dielectric/metal/dielectric transparent electrode," *Opt. Express* **20**(2), 845–853 (2012).

38. T. Schwab et al., "Highly efficient color stable inverted white top-emitting OLEDs with ultra-thin wetting layer top electrodes," *Adv. Opt. Mater.* **1**(10), 707–713 (2013).

39. S. Schubert et al., "Improvement of transparent metal top electrodes for organic solar cell by introducing a high surface energy seed layer," *Adv. Energy Mater.* **3**(4), 438–443 (2013).

40. S. Liu et al., "Silver/germanium/silver: an effective transparent electrode for flexible organic light-emitting devices," *J. Mater. Chem. C* **2**(5), 835–840 (2014).

41. P. Melpignano et al., "E-beam deposited ultra-smooth silver thin film on glass with different nucleation layers: an optimization study for OLED micro-cavity application," *Org. Electron.* **11**(6), 1111–1119 (2010).

42. J. Meiss, M. K. Riede, and K. Leo, "Optimizing the morphology of metal multilayer films for indium tin oxide (ITO)-free inverted organic solar cells," *J. Appl. Phys. Lett.* **105**(6), 063108 (2009).

43. G. W. Hyung et al., "Bottom-emission organic light-emitting diodes using semitransparent anode electrode by O2 plasma," *Org. Electron.* **13**(11), 2594–2599 (2012).

44. T. Schwab et al., "Eliminating micro-cavity effects in white top-emitting OLEDs by ultra-thin metallic top electrodes," *Adv. Opt. Mater.* **1**(12), 921–925 (2013).

45. S. Schubert et al., "Oxide sandwiched metal thin-film electrodes for long-term stable organic solar cells," *Adv. Funct. Mater.* **22**(23), 4993–4999 (2012).

46. H. Cho, J.-M. Choi, and S. Yoo, "Highly transparent organic light-emitting diodes with a metallic top electrode: the dual role of a Cs_2CO_3 layer," *Opt. Express* **19**(2), 1113–1121 (2011).

47. W. Wang et al., "Transparent ultrathin oxygen-doped silver electrodes for flexible organic solar cells," *Adv. Funct. Mater.* **24**(11), 1551–1561 (2014).

48. C. Zhang et al., "An ultrathin, smooth, and low-loss al-doped Ag film and its application as a transparent electrode in organic photovoltaics," *Adv. Mater.* **26**(32), 5696–5701 (2014).

49. D. Gu et al., "Ultrasmooth and thermally stable silver-based thin films with subnanometer roughness by aluminum doping," *ACS. Nano* **8**(10), 10343–10351 (2014).

50. J. Salinas et al., "Optical design of transparent thin metal electrodes to enhance in-coupling and trapping of light in flexible polymer solar cells," *Adv. Mater.* **24**(47), 6362–6367 (2012).

51. S. Kim et al., "Design of red, green, blue transparent electrodes for flexible optical devices," *Opt. Express* **22**(S5), 1257–1269 (2014).

52. S. Kim and J.-L. Lee, "Design of dielectric/metal/dielectric transparent electrode for flexible electronics," *J. Photon. Energy* **2**(1), 021215 (2012).

53. K. Hong and J.-L. Lee, "Inverted top-emitting organic light-emitting diodes using transparent silver oxide anode formed by oxygen plasma," *Electrochem. Solid State Lett.* **11**(2), H29–H31 (2008).

54. Z. B. Wang et al., "Unlocking the full potential of organic light-emitting diodes on flexible plastic," *Nat. Photon.* **5**, 753–757 (2011).

55. H. A. Macleod, *Thin-Film Optical Filters*, pp. 64, Thin Film Center, Arizona (1986).

56. V. Bulovic et al., "Weak microcavity effects in organic light-emitting devices," *Phys. Rev. B* **58**, 3730–3740 (1998).

57. H. C. Kim, T. L. Alford, and D. R. Allee, "Thickness dependence on the thermal stability of silver thin films," *Appl. Phys. Lett.* **81**(22), 4287–4289 (2002).

58. K. Thurmer, E. D. Williams, and J. E. Reutt-Rovey, "Dewetting dynamics of ultrathin silver films on Si(111)," *Phys. Rev. B* **68**, 155423 (2003).

59. N. Kaiser, "Review of the fundamentals of thin-film growth," *Appl. Opt.* **41**(16), 3053–3060 (2002).

60. C. T. Campbell, "Ultrathin metal films and particles on oxide surface: structural, electronic and chemisorptive properties," *Surf. Sci. Rep.* **27**(1–3), 1–111 (1997).

61. K. Hong et al., "Design rules for highly transparent electrodes using dielectric constant matching of metal oxide with Ag film in optoelectronic devices," *Chem. Commun.* **48**(86), 10606–10608 (2012).

62. E. A. Coronado, E. R. Encina, and F. D. Stefani, "Optical properties of metallic nanoparticles: manipulating light, heat and forces at the nanoscale," *Nanoscale* **3**(10), 4042–4059 (2011).
63. G. H. Jung et al., "BCP/Ag/MoO$_3$ transparent cathodes for organic photovoltaics," *Adv. Energy Mater.* **1**(6), 1023–1028 (2011).
64. L. Vitos et al., "The surface energy of metals," *Surf. Sci.* **411**(1–2), 186–202 (1998).
65. V. J. Logeeswaran et al., "Ultrasmooth silver thin films deposited with a germanium nucleation layer," *Nano Lett.* **9**(1), 178–182 (2009).
66. C. Cioarec et al., "Ultrasmooth silver thin film electrodes with high polar liquid wettability for OLED microcavity application," *Langmuir* **27**(7), 3611–3617 (2011).
67. E. G. Seebauer and C. E. Allen, "Estimating surface diffusion coefficients," *Prog. Surf. Sci.* **49**(3), 265–330 (1995).
68. H. M. Stec et al., "Ultrathin transparent Au electrodes for organic photovoltaics fabricated using a mixed mono-molecular nucleation layer," *Adv. Funct. Mater.* **21**(9), 1709–1716 (2011).
69. J. Zou et al., "Interfacial engineering of ultrathin metal film transparent electrode for flexible organic photovoltaic cells," *Adv. Mater.* **26**(22), 3618–3623 (2014).
70. H. C. Kim, T. L. Alford, and D. R. Allee, "Thickness dependence on the thermal stability of silver thin films," *Appl. Phys. Lett.* **81**, 4287 (2002).
71. J. H. Son et al., "Effect of reflective P-type ohmic contact on thermal reliability of vertical InGaN/GaN LEDs," *Electron. Mater. Lett.* **10**(6), 1171–1174 (2014).
72. R. S. Sennett and G. D. Scott, "The structure of evaporated metal films and their optical properties," *J. Opt. Soc. Am.* **40**(4), 203–211 (1950).
73. A. E. B. Presland, G. L. Price, and D. L. Trimn, "Kinetics of hillock and island formation during annealing of thin silver films," *Prog. Surf. Sci.* **3**(1), 63–96 (1972).
74. R. E. Hummel and H. J. Geier, "Activation energy for electrotransport in thin silver and gold films," *Thin Solid Films* **25**(2), 335–342 (1975).
75. N. P. Sergeant et al., "Design of transparent anodes for resonant cavity enhanced light harvesting in organic solar cells," *Adv. Mater.* **24**(6), 728–732 (2012).
76. H. Yu et al., "Quantitative determination of the metastability of flat Ag overlayers on GaAs (110)," *Phys. Rev. Lett.* **88**(1), 016102 (2001).
77. H. Krishna et al., "Thickness-dependent spontaneous dewetting morphology of ultrathin Ag films," *Nanotechnology* **21**(15), 155601 (2010).
78. S. Hofmann et al., "Top-emitting organic light-emitting diodes," *Opt. Express* **19**(S6), A1250–A1264 (2011).
79. P. Freitag et al., "White top-emitting organic light-emitting diodes with forward directed emission and high color quality," *Org. Electron.* **11**(10), 1676–1682 (2010).

Illhwan Lee received his BS degree in materials science and engineering from Hanyang University in 2009 and his MS degree in materials science and engineering from POSTECH in 2011. He is currently a PhD candidate in Professor Jong-Lam Lee's research group at POSTECH. His research interests include design of flexible transparent electrodes and architecture of nanostructured light out-coupling layers for optical devices.

Jong-Lam Lee received a PhD degree in materials science and engineering from KAIST in 1985. He joined POSTECH in 1996. He is heading the Department of Materials Science and Engineering and was selected as a POSTECH fellow. His research covers architecture of nanostructures for photon extraction, flexible substrates for printing processes of flexible displays, and design of photonic devices. He published more than 300 papers in academic journals.